Physica Medica 64 (2019) 195–203

Contents lists available at ScienceDirect

Physica Medica

journal homepage: www.elsevier.com/locate/ejmp

Original paper

Experimental characterisation of a proton kernel model for pencil beam scanning techniques

L. De Marzi[a,b,*], A. Da Fonseca[a], C. Moignier[a], A. Patriarca[a], F. Goudjil[a], A. Mazal[a], I. Buvat[c], J. Hérault[d]

[a] Institut Curie, Radiation Oncology Department, Centre de protonthérapie d'Orsay, Orsay, France
[b] Institut Curie, University Paris Saclay, PSL Research University, Inserm U 1021-CNRS UMR 3347, Orsay, France
[c] CEA – IMIV, U1023 Inserm/CEA/ERL 9218 CNRS, SHFJ, Orsay, France
[d] Centre Antoine Lacassagne, Nice, France

ARTICLE INFO

Keywords:
Proton therapy
Pencil beam scanning
Monte Carlo
Geant4

ABSTRACT

The aim of this work is to perform Monte Carlo simulations of a proton pencil beam scanning machine, characterise the low-dose envelope of scanned proton beams and assess the differences between various approximations for nozzle geometry. Measurements and Monte Carlo simulations were carried out in order to describe the dose distribution of a proton pencil beam in water for energies between 100 and 220 MeV. Dose distributions were simulated by using a Geant4 Monte Carlo platform (TOPAS), and were measured in water using a two-dimensional ion chamber array detector. The beam source in air was adjusted for each configuration. Double Gaussian parameterisation was proposed for definition of the beam source model in order to improve simulations starting at the nozzle exit. Absolute dose distributions and field size factors were measured and compared with simulations. The influence of the high-density components present in the treatment nozzle was also investigated by analysis of proton phase spaces at the nozzle exit. An excellent agreement was observed between experimental dose distributions and simulations for energies higher than 160 MeV. However, minor differences were observed between 100 and 160 MeV, suggesting poorer modelling of the beam when the full treatment head was not taken into account. We found that the first ionisation chamber was the main cause of the tail component observed for low proton beam energies. In this work, various parameterisations of proton sources were proposed, thereby allowing reproduction of the low-dose envelope of proton beams and excellent agreement with measured data.

1. Introduction

The pencil beam scanning (PBS) technique consists of magnetically scanning pencil beams over a target volume, with the possibility of adjusting the position, energy, and fluence of the beams. As proton therapy is now part of routine clinical practice in a large number of institutions, considerable research has recently focussed on the development and improvement of dose calculation algorithms and simulation codes [1–3]. The very promising results demonstrated using full Monte Carlo (MC) codes encouraged us to evaluate these techniques for dose calculations in proton therapy, for commissioning and quality assurance of beam delivery and for research purposes, starting with the passive scattering technique [4,5]. As a pencil beam scanning proton therapy unit has recently been commissioned for clinical usage at our facility, we modelled and simulated the beam delivery system, including the nozzle with all beamline elements and magnetic steering. The ability of MC methods to accurately model proton therapy treatments based on full simulations of the entire treatment head, as well as parameterised proton sources at the treatment head exit has been extensively investigated by several teams [6–11]. Indeed, one of the challenges for MC simulation is to decrease the computer calculation time, while maintaining reliable calculations. As the relatively few nozzle elements do not always have a major influence on the beam characteristics in PBS, one can choose between the use of simplified simulations starting at the nozzle exit and simulations with complete transportation of the beam through all components. In any case, modelling of beam source parameters is usually obtained by using a set of measurements performed around the isocentre of the treatment room, which may correspond to the measurements required by treatment planning systems. In clinically relevant energy particle beams

* Corresponding author at: Institut Curie, Radiation Oncology Department, Centre de protonthérapie d'Orsay, Orsay, France.
E-mail address: ludovic.demarzi@curie.fr (L. De Marzi).

https://doi.org/10.1016/j.ejmp.2019.07.013
Received 5 December 2018; Received in revised form 20 June 2019; Accepted 17 July 2019
Available online 23 July 2019

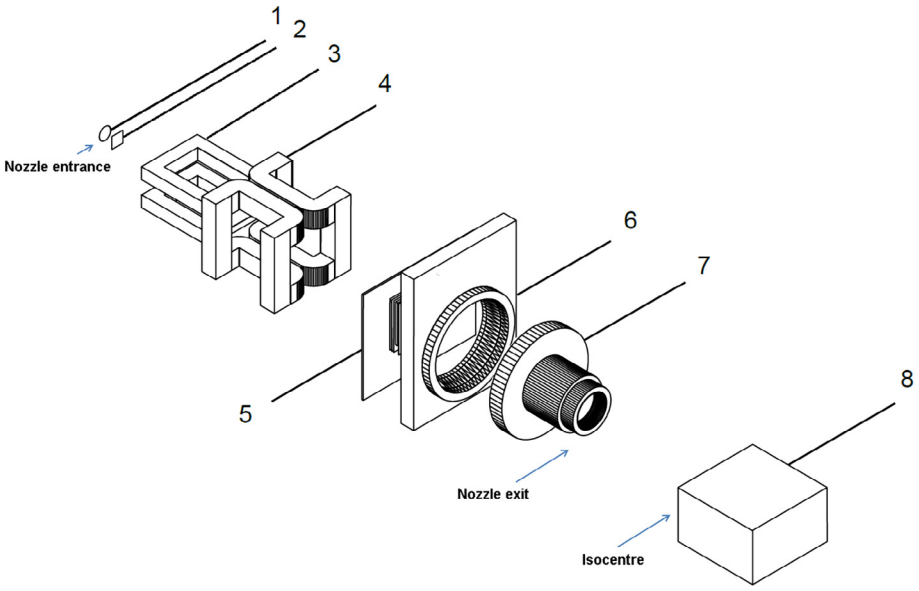

Fig. 1. ICPO proton beam line used for pencil beam scanning as built in TOPAS. Shown are (1) the exit window, (2) first ion chamber, (3)-(4) scanning magnets, (5) second ion chamber, (6–7) snout holder and snout, (8) water tank (the isocentre is located at the surface of the water tank). The source planes where the beam source models were parameterised for the two nozzle geometries (nozzle entrance and nozzle exit) are also indicated.

(60–250 MeV) and individual pencil beams, the lateral dose distribution may be described by a core that consists of primary protons, laterally surrounded by a low-dose envelope. This tail is due to large-angle scattered particles produced by nuclear interactions or large-angle Coulomb scattering of primary particles. As reported by [4] and [12], the low-dose envelope in air, related to scattering of protons in a multi-wire profile monitor, is more significant for low-energy beams and therefore depends on the design of the beamline components. [13] studied the two-dimensional spot profiles for two different nozzles (universal nozzle equipped with double scattering and pencil beam scanning, or PBS-dedicated nozzle) and reported a slight increase of the low-dose envelope in air for the universal nozzle. As described by many groups, secondary particles produced in matter are also significant contributors to the low-dose envelope, particularly for clinically relevant energy beams: many analytical approximations or fitting procedures have been described to determine the extent of the beam halo for treatment planning systems. For protons, the lateral dose profile of a pencil beam in water is typically modelled as several superimposed functions fitted with measured or simulated data. A first component (generally a single or double-Gaussian function) describes the fluence in air and the Coulomb multiple scattering of primary particles, while the functional form of the beam nuclear halo can be described by the addition of one or two other Gaussian distributions [14–17] or a modified Cauchy-Lorentz function [18,19]. [20] and [21] also discussed and put in perspective the impact on dose calculations of using an increased complexity for beam modelling. A detailed description of the various components that constitute the dose distribution of a pencil beam has recently been proposed [22], together with an accurate comparison between measurements and MC simulations with Geant4 for a 177 MeV proton beam in water [23]. Excellent agreement was obtained between simulations and measurements, justifying the use of Geant4 and its nuclear models for PBS calculations.

The aim of this work was therefore to:

- Assess the differences between simulation of the entire treatment nozzle geometry and parameterisation of the beam at the treatment nozzle exit.
- Characterise the low-dose envelope of scanned proton beams.
- Perform Monte Carlo simulation of our proton pencil beam scanning machine, and benchmark the results of simulation with measured data obtained during commissioning of the system.

Measurements and Monte Carlo simulations were therefore carried out to model the dose distribution of proton pencil beams in water. Dose distributions were simulated using a widespread Geant4-based Monte Carlo platform and measured in a water tank using a commercial two-dimensional ion chamber array detector (MatriXX, Ion Beam Applications (IBA) Dosimetry) and a Bragg peak chamber. Simulations and measurements were compared for a wide range of energies, paying particular attention to the low-dose envelope area of the pencil beams.

2. Materials and methods

2.1. Monte Carlo simulations

A MC simulation code based on Geant4 toolkit was parameterised and benchmarked in this study, as simulations of an IBA system in beam scanning mode were already proposed with this code, albeit with slight differences in methodology. Two parameterisations of proton source were compared, with various approximations for nozzle geometry (a simulation of the entire treatment nozzle geometry, and a parameterisation of the beam at the treatment nozzle exit). The toolkit was TOPAS (TOolkit for PArticle Simulation, [24], v3.1.p2 with Geant4.10.03p01), a software environment that allows simulation of full particle therapy systems, which is tailored to proton therapy applications. TOPAS has already been used to model and simulate the Massachusetts General Hospital (MGH) full treatment head in beam scanning mode [10]. Since our gantry is very similar to that installed at MGH, we updated the geometry of the delivery system in TOPAS to the IBA gantry installed at our institution. All elements composing the nozzle (particularly the vacuum window (VW) located 290 cm from the isocentre, the first and second ionisation chambers (IC) located 283 and 116 cm upstream from the isocentre, the scanning magnets (SM) located 193 and 233 cm upstream from the isocentre, the movable jaws (MJ), and the snout (SN)) were taken into account according to the manufacturer's blueprints and technical data. Fig. 1 shows the beam line used for PBS as built in TOPAS. The distances between the isocentre, the monitor chamber, the scanning magnets and the vacuum window were adjusted to our nozzle geometry. The geometrical models for the two ionisation chambers were also accurately adjusted. The first chamber (IC1) at nozzle entrance consists of parallel electrodes, horizontal and vertical tungsten wires (25 μm diameter), a mylar foil coated with both sided Aluminum, and two kapton windows. This chamber monitors the beam spot size and shape. The second segmented transmission chamber (IC2), contains two independent components with mylar foils coated with both sided Aluminum strips, monitors the

beam position and uniformity and determines the beam output factor.

The "emittance" source type was used with "BiGaussian" distribution name, providing a way of sampling particles' position (σ_X and σ_Y) and momentum direction (σ_X' and σ_Y') on a plane (Gaussian distributions were assumed for the position and momentum direction), as well as the specification of a correlation factor between σ_X and σ_X', and σ_Y and σ_Y'. As the coefficient of correlation is positive for a defocusing beam and negative for a focusing beam, the source parameters were optimised with negative correlation values for the simulations starting at the nozzle entrance (to mimic the focusing effect of the quadrupoles) and positive values for the simulations starting at the nozzle exit. Manual optimisation of width of the Gaussian distributions were performed in order to obtain a good agreement between measurements and simulated data, and to reproduce the overall beam emittance. The source planes where the beam source model was parameterised for the two nozzle geometries were located 290 cm and 50 cm from the isocentre for simulations starting at the nozzle entrance and nozzle exit respectively (see Fig. 1). For beam steering, we adopted the method described by [6] and used uniform magnetic fields within the scanning magnets (with "classical 4th order Runge-Kutta" stepping algorithm), while omitting the quadrupole magnets. The TOPAS simulations were run with a physics list composed of seven modules: "tsem-standard opt3 WVI", "g4h-phy QGSP BIC HP", "g4decay", "g4ion-binarycascade", "g4h-elastic HP", "g4stopping", "g4radioactivedecay", as already proposed for proton therapy [25]. Ionisation potentials of 80 eV for water and 85.7 eV for air, respectively, were employed. Cuts for all particle productions were set to 0.05 mm and the dose scoring grid resolution was $1 \times 1 \times 1\,mm^3$. In all simulations, the parameters for the minimum and maximum EM range were set to 100 eV and 230 MeV, the number of bins per decade for stopping power and lambda bins were set to 100. All other parameters used default options and a total of $1x10^8$ proton histories per pencil beam were simulated for each setup. The average computation time was ranging between 153 h and 320 h on a single CPU depending on the beam energy and geometry configuration (a factor of two was found between the full nozzle and nozzle exit simulations). The simulations were run on a multiprocessor Linux cluster of 128 CPUs.

2.2. Measurements and source parameters adjustments

In our facility, we use a 230 MeV proton cyclotron (IBA, Belgium), delivering the beam to a universal nozzle-equipped gantry and two fixed horizontal beamlines. In the context of PBS commissioning for our treatment planning system (TPS), beam data library measurements were performed for a wide range of energies and geometries around the isocentre of the treatment room. Pencil beams or spots are defined as elementary quasi-monoenergetic proton beams with a small size Gaussian-like shape, typically with standard deviations (σ) of a few millimetres. Among the experimental data, integral depth-dose profiles (IDD) and spot sizes in air ($\sigma_{x,y}$ corresponding to the standard deviation of the Gaussian primary beam in x or y axes) at five distances around the isocentre (from −20 to +20 cm) were measured. The IDDs were measured with a Bragg Peak Chamber (type 34070, PTW, diameter of 81.6 mm) in a water tank. The diameter of the detector was taken into account in the simulations but the chamber was not simulated (we scored the energy deposited in a 40.8 mm radius cylindrical volume placed in water with depth bin thickness of 0.5 mm as described in [26]). The spot sizes in air were measured using a two-dimensional detector (scintillator screen with a LYNX CCD camera, Fimel, $0.5 \times 0.5\,mm^2$ resolution) for energies between 100 and 226.9 MeV in 5 MeV steps, and were compared for two gantry angles (at 0° and 270°, the latter being considered as the reference). As the pencil beam must be as symmetrical as possible around the isocentre plane, beam asymmetry is acceptable within the treatment volume, but can vary upstream and downstream to the isocentre. Two-dimensional elliptical Gaussian functions were fitted to the measurements to obtain spot size and momentum parameterisations. The orientation of the Gaussian distribution and the resulting $\sigma_{x,y}$ values for the spot sizes were obtained by averaging the major and minor axes of the (rotated elliptical) spots that do not always coincide with the x and y axes (Eqs. (1a) and (1b)). For simplicity, we then neglected possible differences between σ_x and σ_y, and the average of spot sizes in the x and y directions σ_1 was used to adjust the MC source parameters to our beamline (see Eq. (1a)).

$$F(X,Y) = \exp(-[a(x-x_0)^2 + b(x-x_0)(y-y_0) + c(y-y_0)^2]) \approx \exp\left(\frac{-[(x-x_0)^2 + (y-y_0)^2]}{2\sigma_1^2}\right) \quad (1a)$$

With the following definitions:

$$a = \left(\frac{\cos^2(\theta)}{2\sigma_X^2} + \frac{\sin^2(\theta)}{2\sigma_Y^2}\right)$$
$$b = \left(\frac{\sin(2\theta)}{2\sigma_X^2} - \frac{\sin(2\theta)}{2\sigma_Y^2}\right)$$
$$c = \left(\frac{\sin^2(\theta)}{2\sigma_X^2} + \frac{\cos^2(\theta)}{2\sigma_Y^2}\right) \quad (1b)$$

where (x_0,y_0) are the coordinates of the pencil beam axis, $\sigma_{x,y}$ or σ_1 describes the lateral spread of the beam source.

In order to characterise the low-dose envelope at the sub-percent level, the central and tail regions of the beam were obtained in air around the isocenter by employing the pair/magnification technique described in [27], which consists in merging two sets of images with different exposure and saturation levels. The experimental data were used to define the source description files of both MC simulations (starting at the nozzle exit or with full nozzle modelling) after having derived the useful beam parameters by linear interpolations or third-order polynomial fitting (mean energy, energy spread, beam size in air, divergence, and emittance). We followed the detailed procedures described in [7,10], in particular with regard to the following points:

- the mean energy value E at the entrance of each simulation was adjusted in the Monte Carlo codes in order to have the same range as the measurement (defined at the distal 80% of the maximum dose value).
- the energy spread was determined to obtain the best agreement between measured and simulated peak widths and peak-to-plateau ratio.
- the beam size in air (primary and secondary components) were extrapolated at the entrance of each simulation (290 cm and 50 cm from the isocentre for simulations starting at the nozzle entrance and nozzle exit respectively).
- the beam emittance was set to half the beam size times the beam divergence times π.

The MC simulations of our beamline were then benchmarked with the measurements, and validated by comparing measured and simulated spot sizes at the isocentre in air. Spot sizes in the presence of a 6.5 cm range shifter (a slab of PMMA material inserted in the beam path to enable treatment in shallow depth) were measured and compared to simulations for various air-gaps. To evaluate the dosimetric contribution of the low-dose envelope at the centre of large fields (comprising a large number of pencil beams), field size factors (FSF) were also measured in water at several depths and energies for square fields ranging from 2x2 to 10x10 cm^2. The fields consisted of 64 to 1225 regularly spaced (3 mm) pencil beams, and the field size factors were defined as the ratio of the dose at the centre of a given field to the dose at the centre of the 10x10 cm^2 field. The results were compared with MC simulations in order to validate the model in the case of scanned fields.

2.3. Low-dose envelope characterisation

To study the relative impact of the high-density components present

in the treatment nozzle and to derive the origin of the halo component in air, four simulations (including the IBA nozzle and the air contribution) were compared:

- with no ionisation chamber included in the IBA nozzle,
- with only the first ionisation chamber IC1 included in the IBA nozzle,
- with only the second ionisation chamber IC2 included in the IBA nozzle,
- with full nozzle geometry.

The TOPAS phase space scorer was used to compare the particle properties at the nozzle exit between simplified and full geometry simulations, in order to save the position, energy and momentum of the particles constituting the pencil beam. The number of particles as a function of their position along the lateral profile of the pencil beam, as well as the energy spectrum and direction were stored for various proton beam energies between 100 and 220 MeV. The parameters of the spots at the nozzle exit were compared with and without simulating the chambers, and the parameters of an equivalent proton source located at the end of the treatment head were then defined. As the fluence of the pencil beam deviates from a single Gaussian function after the nozzle exit, this last step was performed by approximating the source lateral fluence distribution F as two superimposed symmetrical Gaussian functions, expressed by Eq. (2). Optimisation of parameters was performed using the Matlab® computing environment (Version R2018a, Mathworks, Natik, MA) with a standard weighted Chi-square minimisation algorithm (Levenberg-Marquardt gradient method) in order to get matching of spot profiles between the full nozzle and nozzle-exit geometry simulations at the isocentre. To obtain the spread and weights of the two distinct components after the nozzle exit, the first Gaussian parameter σ_1 was estimated separately, and then used as starting point during the optimisation process with other parameters set to 0 as a start. We verified that different initial points would not have altered the result of the fit.

$$F(X, Y) = (1 - a_2)\exp\left(\frac{-[(x - x_0)^2 + (y - y_0)^2]}{2\sigma_1^2}\right) + a_2 \exp\left(\frac{-[(x - x_0)^2 + (y - y_0)^2]}{2\sigma_2^2}\right) \quad (2)$$

where (x_0,y_0) are the coordinates of the pencil beam axis, $\sigma_{1,2}$ describes the lateral spread of the beam source and $(1\text{-}a_2)$ and a_2 are the weight of the distinct components.

2D transversal dose distributions for single pencil beams in water were subsequently measured using MatriXX with its water phantom and electrometer (DigiPhant, IBA dosimetry), consisting of a matrix of 1020 chambers (0.032 cm^3 collection volume, internal diameter 4.5 mm) in a $32 \times 32\ cm^2$ grid with 7.62 mm centre-to-centre distance. 2D transversal distributions were acquired with 1–5 mm depth resolution (adapted to the dose variations along the Bragg peak) and the same number of monitor units at each depth (10 MU), and compared with energy simulations between 100 and 220 MeV in 20 MeV steps. Lateral profiles were compared using a 1 mm distance to agreement (DTA) criterion.

3. Results

3.1. Beam modelling

The proton entrance energy E was optimised to reproduce the experimentally determined range of the beam in water: a relation between the energy at the nozzle entrance E and the energy at the nozzle exit E_0 was then derived (Table 1a). The third-order polynomial used to describe the energy spread relationship is given in Table 1a. The best energy spread values as a function of the initial energy are shown in Fig. 2. Fig. 3 shows the comparison of integral Bragg peaks (IDDs) obtained for several energies after fitting of the parameters with experimental data. The dose agreement between depth-dose measurements in water and simulation data was within ± 2% for both simulations, taking into account the limited diameter of the chamber. The mean point-to-point dose differences were 0.2, 0.8, 0.1%, and −0.6, 0.5, 0.1% for the nozzle exit and nozzle entrance conditions at 100, 160, and 220 MeV, respectively.

Experimental spot sizes as a function of energy E_0 (in MeV) for two gantry angles (0° and 270°), at the nozzle exit and at the isocentre, are represented in Fig. 4a. Error bars represent the differences between major and minor axes of the spots. These differences range between 5% at 100 MeV and up to 9% at 220 MeV. In addition, a spot size variation at the isocentre less than 8% was also found between different gantry angles. Beam properties are described in terms of spot positions (σX and σY), beam momentum (σX′ and σY′), and energy spread (σE): the fitted parameters of the third-order polynomial functions used to describe the relationships between spot size and optical beam properties with energy are shown in Table 1 for both simulation codes. The mean deviation between simulated and calculated primary spot sizes at isocentre in air was 0.2 ± 0.07 mm.

Fig. 4b and Table 1 shows the variation of experimental primary and secondary spot sizes in air as a function of energy E_0, as well as the parameterisation of the long-tail measurement. Table 1b shows the weight and spread of the first and second proton source distributions (see Eq. (2)) for different beam energies, in air at the isocentre. Adding a second Gaussian component with a wider standard deviation to the pencil beam source improved the agreement between simulated and experimental data in the low-dose envelope region up to the 0.01% isodoses, for simulations starting after the nozzle exit.

Fig. 5 shows the variation of experimental and simulated spot sizes along the beam axis for different positions of the RS (airgap = RS-to-isocentre distance from 10 to 30 cm) and proton beam energies. The simulated spot sizes closely matched those measured downstream of the RS: the absolute point-to-point differences between experimental and simulated spot size were within ± 0.3 mm, with a mean ± standard deviation difference of −0.05 ± 0.15 mm.

3.2. Low-dose envelope characterisation

Fig. 6 presents the comparison of simulated and experimental data for a perpendicularly incident pencil beam on a water phantom for three different energies. Lateral profiles were compared for the two MC models (starting at the nozzle exit or at the nozzle entrance, respectively). As shown in Fig. 6, an excellent agreement was observed between the experimental dose profiles and the simulations starting from the nozzle exit (within 1 mm DTA over 4 orders of magnitude for lateral dose profiles) for energies higher than 160 MeV, as also observed in [23] at 177 MeV. However, minor differences were observed at 100 MeV (66% and 93% of points pass the criteria of 1 mm DTA for dose levels as low as 0.01% and 0.1% of the central dose respectively), suggesting poorer modelling of the beam halo for that range of energies and in very low dose regions (< 0.1% dose level). The agreement between experimental and simulated data for simulation with the entire nozzle geometry was also very good, particularly at low energies: the DTA is within 1 mm for all dose levels as low as 0.01%, precisely reproduced for the whole range of energies.

Field size factor values were measured for three different beam energies at several depths and were compared with MC simulations (nozzle exit and full nozzle geometry): the results are presented in Fig. 7, in which dose measurements and MC calculations are plotted against depth, and FSF are plotted against field sizes ranging from 2x2 to 10x10 cm^2. Very good agreement was observed between measured and simulated FSFs for all energies and all field sizes: MC simulations starting at the nozzle exit predicted the increase and dependency of FSF

Table 1
(a) Polynomial functions of description files used for MC simulations with TOPAS Geant4 platform (beam parameters and at the nozzle entrance), for an IBA universal pencil beam scanning nozzle (UN). (b) Proton beam source parameters at the nozzle exit of the IBA universal pencil beam scanning nozzle, approximated by two Gaussian functions, at the isocentre, with σ_1, σ_2 and a_2 the parameters of the distinct components of equation (2).

(a)

	Source Description at the nozzle entrance
Spot size (mm)	$\sigma_x = \sigma_y = 7.5 \times 10^{-5}\ E_0^2 - 9.3 \times 10^{-2}\ E_0 + 19.6$
Spot divergence (mrad)	$\sigma_x' = \sigma_y' = 1.79 \times 10^{-10}\ E_0^3 - 7.8 \times 10^{-8}\ E_0^2 - 9.2 \times 10^{-6}\ E_0 + 4.8 \times 10^{-3}$
Spot correlation	$R_x = R_y = 2.1 \times 10^{-7}\ E_0^3 - 8.6 \times 10^{-5}\ E_0^2 + 1.2 \times 10^{-2}\ E_0 - 1.56$
Energy spread (MeV)	$\sigma_E = -6.5 \times 10^{-7}\ E_0^3 + 2.4 \times 10^{-4}\ E_0^2 - 0.024\ E_0 + 1.40$
Entrance energy (MeV)	$E = 0.9991\ E_0 + 1.676$
	Source Description at the nozzle exit
Primary spot size (mm)	$\sigma_x = \sigma_y = 5.2 \times 10^{-5}\ E_0^2 - 0.042\ E_0 + 9.2$
Secondary spot size (mm)	$\sigma_x = \sigma_y = 5.4 \times 10^{-6}\ E_0^3 - 0.0025\ E_0^2 + 0.291\ E_0 + 3.7$
Primary spot divergence (mrad)	$\sigma_x' = \sigma_y' = -2 \times 10^{-9}\ E_0^3 + 1.14 \times 10^{-6}\ E_0^2 - 2.2 \times 10^{-4}\ E_0 + 0.016$
Secondary spot divergence (mrad)	$\sigma_x' = \sigma_y' = -1.6 \times 10^{-9}\ E_0^3 + 7.9 \times 10^{-6}\ E_0^2 - 1.3 \times 10^{-3}\ E_0 + 0.071$
Spot correlation	$R_x = R_y = 1$
Energy spread (MeV)	$\sigma_E = -6.5 \times 10^{-7}\ E_0^3 + 2.4 \times 10^{-4}\ E_0^2 - 0.024\ E_0 + 1.40$

(b)

Energy E_0	σ_1 (mm)	σ_2 (mm)	σ_1/σ_2	a_2 (%)
100 MeV	7.1	14.9	2.1	2.7
160 MeV	4.8	9.3	1.9	2.6
220 MeV	3.4	5.2	1.5	2.6

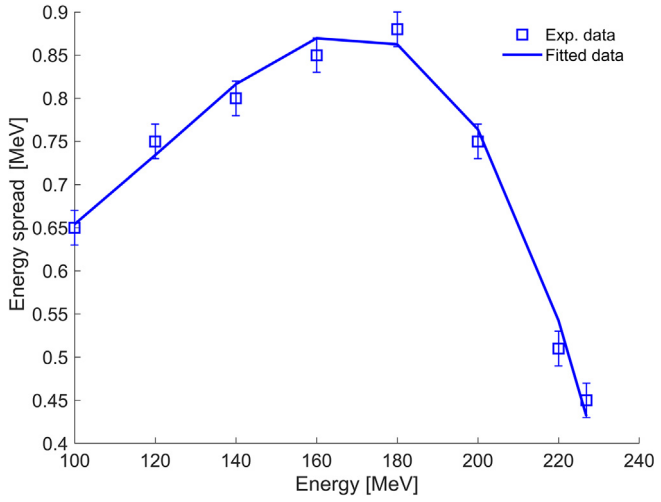

Fig. 2. Best energy spreads estimation (given in MeV) obtained with a 0.02 MeV step. The line represents a cubic polynomial fit as a function of the initial energy.

with field size and depth to within 1.5%, particularly at energies higher than 160 MeV. For field sizes larger than $3 \times 3\,cm^2$, the agreement between the two MC simulations was also similar, whereas, as expected, the agreement with measurements for the smallest field size was slightly better when full nozzle geometry was taken into account. At 100 MeV and due to poorer modelling of the tail component, deviations below 2.5% were observed between nozzle exit simulations and measurements.

In order to characterise the low-dose envelope of individual pencil beams after passing through the nozzle, the influence of the two ionisation chambers (IC1 and IC2) on the beam energy spectrum, fluence and scattering was investigated by analysing the proton phase spaces at the isocentre. The results, presented in Fig. 8 for the fluence comparison, indicate that the first ionisation chamber IC1 might be a significant cause for the large-angle scattering and tail component observed for the low proton pencil beam energies. Taking IC1 into account (which contains tungsten wires) in the simulation improved the agreement between simulated and measured data (in terms of dose and fluence level) for voxels above the 0.01% values, whereas IC2 had a lesser impact on spot size and halo extension.

4. Discussion and conclusions

In this paper, we present the modelling results of our proton pencil beam scanning machine, largely based on characterisation of a proton kernel model. MC simulations based on Geant4 were parameterised and compared after various approximations for nozzle geometry, and demonstrated excellent agreement with measured data over the entire energy range, in terms of spot size, and lateral and in-depth profiles in water. However, due to variations of spot asymmetry or size fluctuations with gantry angle, uncertainties persist concerning determination of fitted parameters. The dosimetric consequences of pencil beam width variations in pencil beam scanning have been discussed by [28] or [29], and a 10% value for spot size deviation was shown to have small impact on target coverage (using for example a 3 mm-3% γ-index criteria). As the beam was found to be cylindrically symmetrical to within a few percent (our results are in broad agreement with the gantry angle dependencies of the PBS beam assessed by [29]), the beam properties were assumed to be symmetrical for the MC simulations in this study. As the exact extent of the contribution of large scattering angles to the pencil beam profile is not properly described by models and cannot be assessed separately by measurements, we have described an experimental set-up to characterise two-dimensional spot profiles, including the non-Gaussian low-dose tails down to 0.01% of the central dose. Whereas [23] used an experimental beamline to characterise the halo of a 177 MeV proton beam, we used a widely available clinical gantry and compared simulations of the entire nozzle with relative dose measurements in water for a wide range of energies.

Characterisation of the pencil beam profiles usually requires measurements in air at several energies and distances around the isocentre of the treatment room. Scintillating screens or Gafchromic films have an excellent spatial resolution, are often used to measure in-air spot sizes, and have been proved to be good detectors for the measurement of the low-dose envelope of pencil beams [27]. In this study, we used a scintillation detector for in-air sigma parameterisations, and ionisation

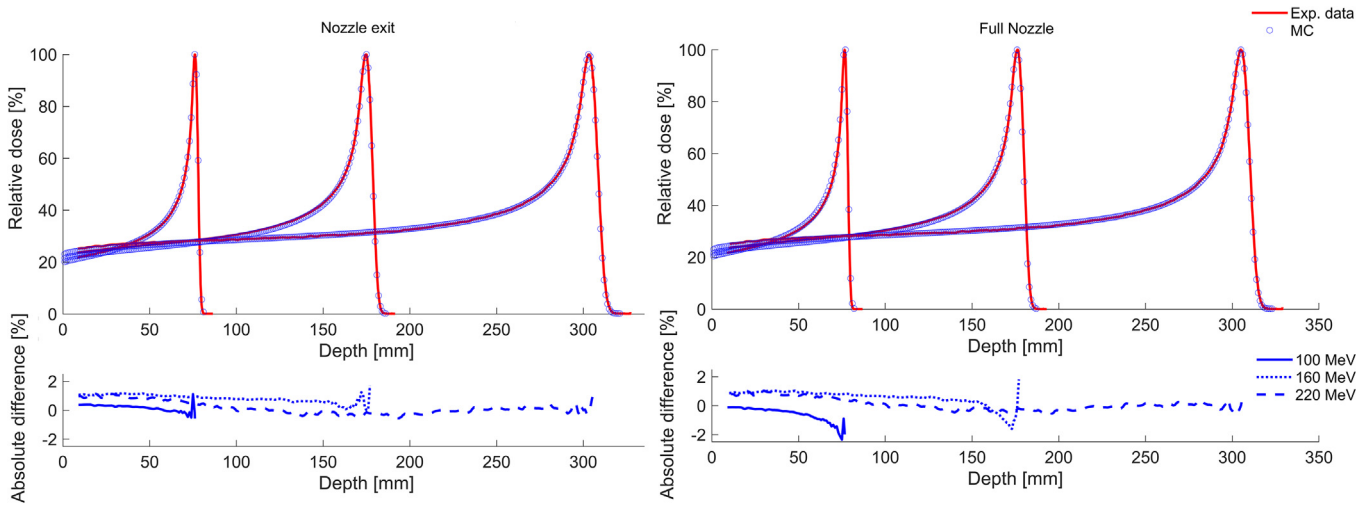

Fig. 3. Measured data obtained during commissioning of the system, and comparisons with MC simulated IDDs in water for three energies (100, 160 and 220 MeV) after optimisation of the beam properties: (a) Comparison between measured data and MC starting at the nozzle exit (b) Comparison between measured data and full nozzle geometry MC.

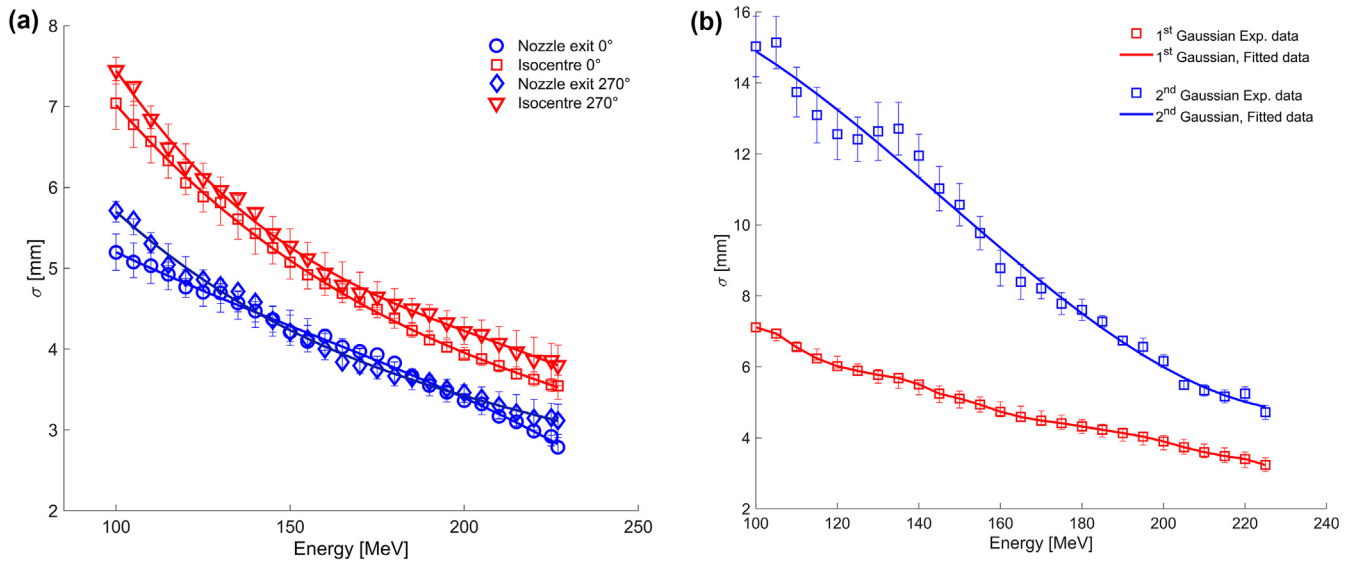

Fig. 4. (a) Variation of experimental primary spot sizes in air as a function of energy for two gantry angles (0° and 270°), at the nozzle exit and at the isocentre (b) Variation of experimental primary and secondary spot sizes in air as a function of energy (270° gantry angle). The solid lines correspond to the fit (see Table 1).

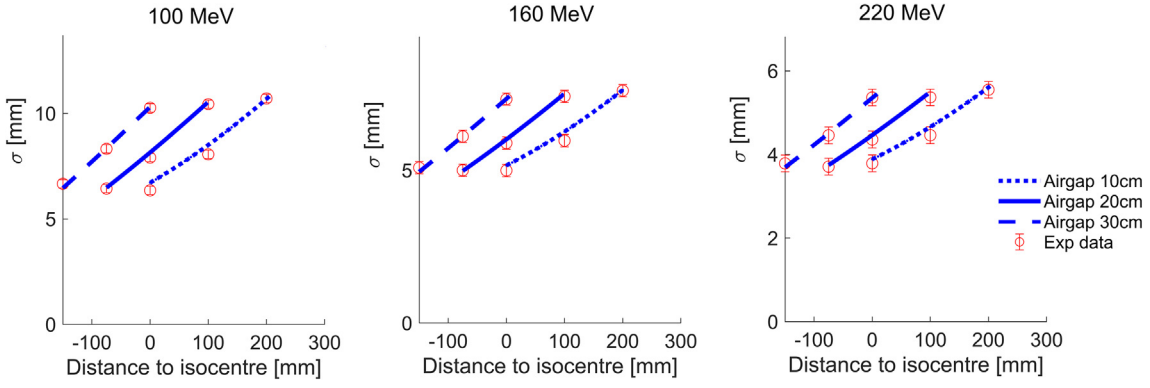

Fig. 5. Comparison of experimentally measured spot sizes (open circles) with those obtained using the MC simulation (lines) for different airgaps and beam energies.

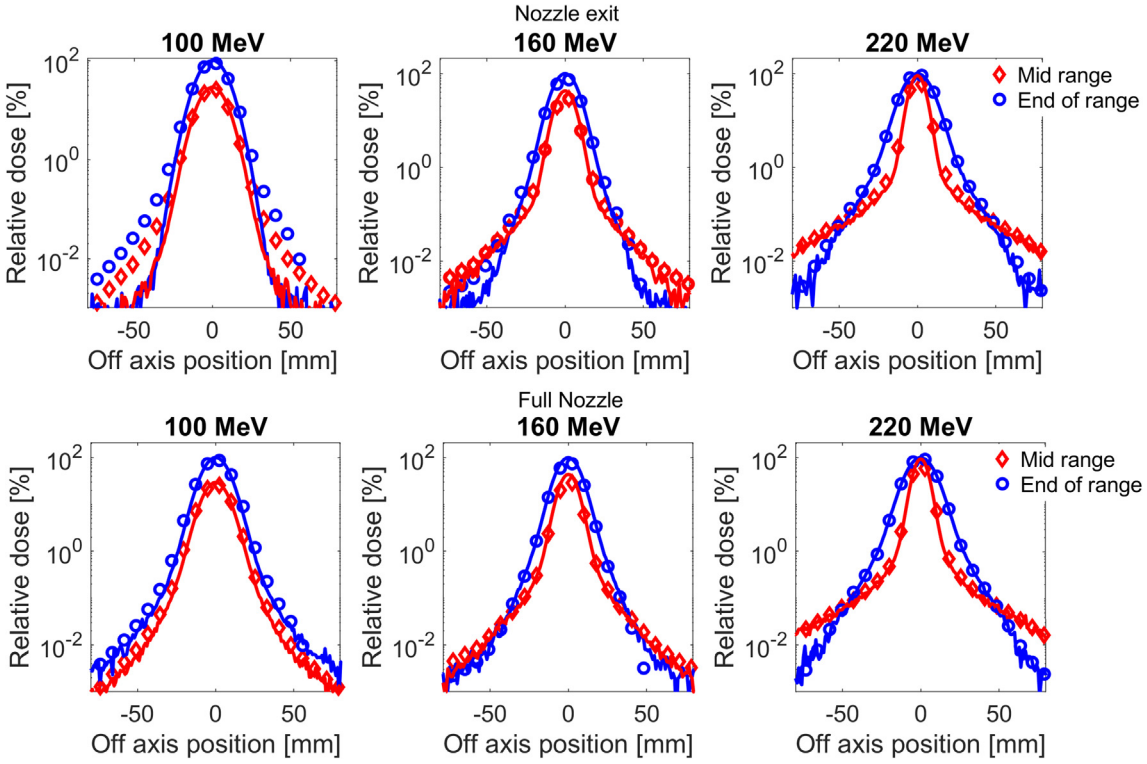

Fig. 6. Dose distribution of a proton pencil beam in water: comparisons of 1D lateral profiles (mid-range and near end of range, experimental data are indicated by open circles) between MC calculations and measurements, for several energies (top figure) MC simulations starting at the nozzle exit (bottom figure) MC simulations with full treatment head modelling.

chambers in water, thereby avoiding the potential under-response of radiochromic films or scintillating screens related to quenching effects for high linear energy transfers. The detector size effect is also fairly small, particularly in the low-dose envelope area, where low dose-gradients are expected.

The range of protons in matter is determined from the stopping power ratio (SPR) of tissues relative to water, and one of the parameters to compute the SPR is the average ionisation potential I. Latest

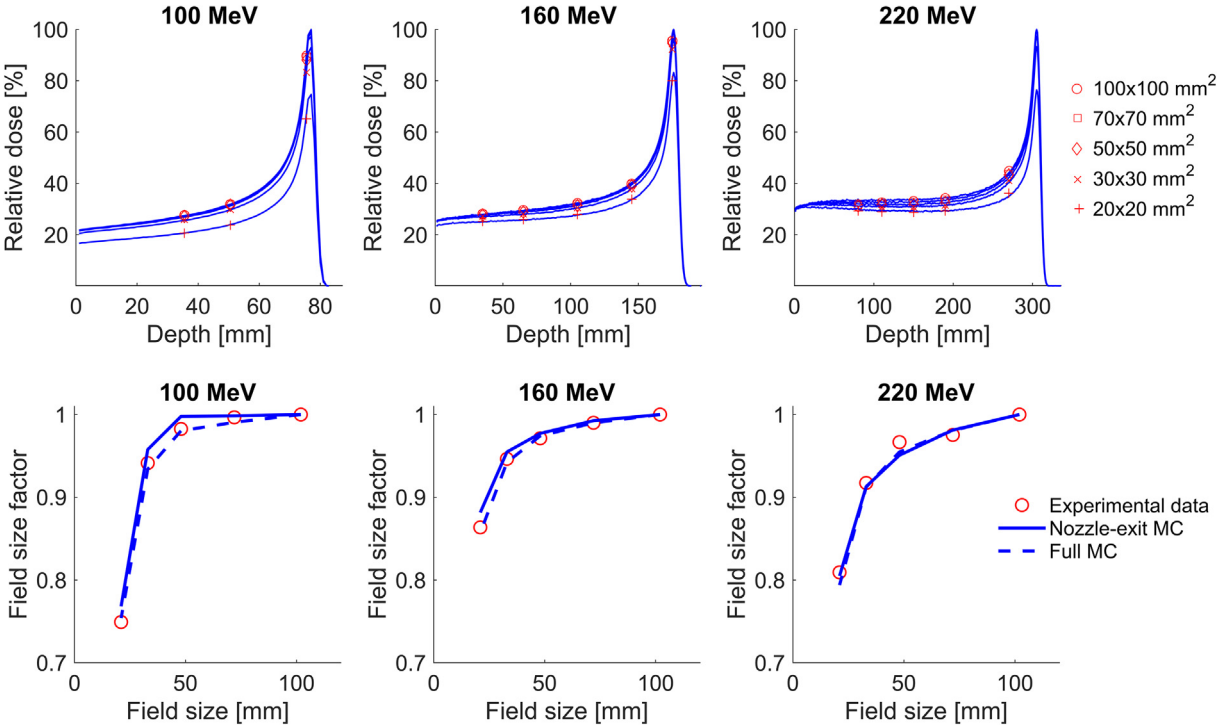

Fig. 7. Simulated (solid/dotted lines) and measured (symbols) IDDs and field size factors on the central axis at various depths (50, 110 and 140 mm at 100, 160 and 220 MeV, respectively) for a proton beam in water.

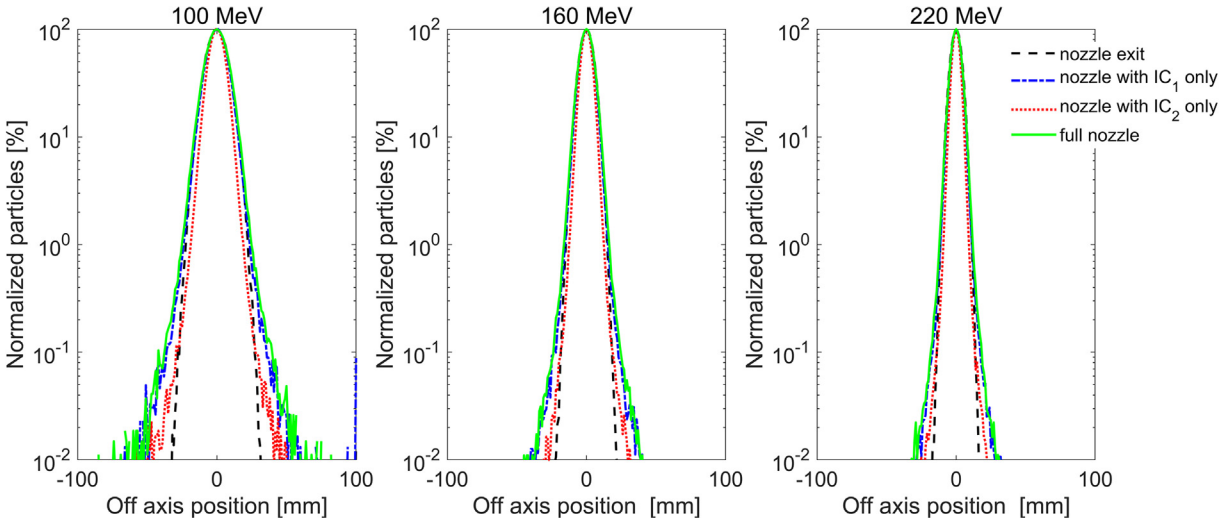

Fig. 8. Comparisons of the lateral fluence at the centre of a pencil beam in air (proton phase spaces analysis at the isocentre), with each of the two ionisation chambers, IC1 and IC2, included in the IBA nozzle, without an ionisation chamber and with the full nozzle geometry.

suggested value by ICRU publications for the ionisation potential for water is 78 ± 2 eV [30], however there is no consensus on how to establish reference value for the I values of tissues. The influence of the uncertainty of the ionisation potential on the proton range has been estimated by many authors: for example [31] estimated that a 10% variation in the elemental I-values introduces a 1.4% variation of the SPR computation. Various sets of stopping power data with I values for air and water between 82.8 and 85.7 eV, and 67.2 and 80.8 eV respectively were compared by [32], resulting in deviations of the order of 1% in the plateau region. In this work, we arbitrary have chosen I values lying within the limits of error quoted in ICRU, identical for all simulations. Indeed, an absolute comparison of the simulated ranges obtained with the various geometries was out of the scope of this study. We decided to use a polynomial fit to calculate the energy required at the entrance of each simulation to achieve the requested range in water at the isocenter, which removes the possible differences in the peak position between the models.

Our results are in broad agreement with previously reported data, particularly in terms of spot size or shapes and field size factors [9,13,16]. After having described an experimental method for determination of the halo component, [26] proposed a modification of the beam source model in MC simulations with a superimposition of Gaussian distributions, thereby allowing reproduction of the low-dose envelope without transporting the beam through the treatment nozzle. With the difference that our results apply to a universal IBA pencil beam scanning nozzle and to simulated data (full MC simulations of the treatment head), the present work provides parameterisation of an equivalent proton source located at the end of the treatment head. Interestingly, Table 1 shows that the weights and standard deviation ratios between first and second components of beam source fluence remain very close as a function of energy. The impact of an improved MC description of the lateral beam profiles on small or extended fields was evaluated in this work, showing that, under certain conditions, large-angle scattering of the beam depends on nozzle geometry and, in particular, originates from the first ionisation chamber high-density components. Indeed these low water-equivalent thickness chambers are composed of thin wires or foils (made of tungsten or aluminium) and can slightly alter beam scattering. As treatment planning system input data or kernel models for lateral and in-depth profiles can sometimes be generated using MC simulation codes [21], accurate modelling of the initial beam fluence or complete description of beamline geometry may be necessary in some cases. For modelling out-of-field doses, a full simulation of the nozzle may also be recommended as discussed in [9]. In this work, we therefore have proposed various parameterisations of equivalent proton sources, allowing reproduction of the halo component of proton pencil beams and excellent agreement with measured data over the entire energy range.

Acknowledgements

The authors acknowledge IBA and Francis H. Burr Proton Therapy Center for sharing beam data measurements and geometry, and Dr. P. Lansonneur for support about graphics views. This work was partly funded by the European Union's Horizon 2020 Research and Innovation programme under Grant Agreement No. 730983, by PRT-K Institut National du Cancer [grant No. 2015-1-RT-06] and by ITMO Cancer AVIESAN (Alliance Nationale pour les Sciences de la Vie et de la Santé, National Alliance for Life Sciences & Health) within the framework of the Cancer Plan [grant No. 18CP117-00].

References

[1] Paganetti H, Jiang H, Parodi K, Slopsema R, Engelsman N. Clinical implementation of full Monte Carlo dose calculation in proton beam therapy. Phys Med Biol 2008;53(17):4825–53.
[2] Jan S, Benoit D, Becheva E, Carlier T, Cassol F, Descourt P, et al. GATE V6 : a major enhancement of the GATE simulation platform enabling modelling of CT and radiotherapy. Phys Med Biol 2011;56(4):881–901.
[3] Sarrut D, Bardiés N, Boussion M, Freud N, Jan S, Létang JM, et al. A review of the use and potential of the GATE Monte Carlo simulation code for radiation therapy and dosimetry applications. Med Phys 2014;41(6):064301.
[4] Stankovskiy A, Kerhoas-Cavata S, Ferrand R, Nauraye C, Demarzi L. Monte Carlo modelling of the treatment line of the proton therapy center in Orsay. Phys Med Biol 2009;54(8):2377–94.
[5] Bonfrate A, Farah J, De Marzi L, Delacroix S, Constant E, Hérault J, et al. Benchmarking Monte Carlo simulations against experimental data in clinically relevant passive scattering proton therapy beamline configurations. Radioprotection 2016;51(2):113–22.
[6] Peterson S, Polf J, Bues M, Ciangaru G, Archambault L, Beddar S, et al. Experimental validation of a Monte Carlo proton therapy nozzle model incorporating magnetically steered protons. Phys Med Biol 2009;54(10):3217–29.
[7] Grevillot L, Bertrand D, Dessy F, Freud N, Sarrut D. A Monte Carlo pencil beam scanning model for proton treatment plan simulation using gate/geant4. Phys Med Biol 2011;56(16):5203–19.
[8] Parodi K, Mairani A, Brons S, Hasch B, Sommerer F, Naumann J, et al. Monte Carlo simulations to support start-up and treatment planning of scanned proton and carbon ion therapy at a synchrotron-based facility. Phys Med Biol 2012;57(12):3759–84.
[9] Grassberger C, Lomax A, Paganetti H. Characterizing a proton beam scanning system for Monte Carlo dose calculation in patients. Phys Med Biol 2015;60(2):633–45.
[10] Fracchiolla F, Lorentini S, Widesott L, Schwarz M. Characterization and validation of a Monte Carlo code for independent dose calculation in proton therapy treatments with pencil beam scanning. Phys Med Biol 2015;60(21):8601–19.

[11] Almhagen E, Boersma DJ, Nyström H, Ahnesjö A. A beam model for focused proton pencil beams. Phys Med: Eur J Med Phys 2018;52:27–32.
[12] Sawakuchi G, Titt U, Mirkovic D, Ciangaru G, Zhu X, Sahoo N, et al. Monte carlo investigation of the low-dose envelope from scanned proton pencil beams. Phys Med Biol 2010;55(3):711–21.
[13] Lin L, Ainsley C, Solberg T, McDonough J. Experimental characterization of two-dimensional spot proles for two proton pencil beam scanning nozzles. Phys Med Biol 2014;59(2):493–504.
[14] Pedroni E, Scheib S, Bóhringer T, Coray A, Grossmann M, Lin S, et al. Experimental characterization and physical modelling of the dose distribution of scanned proton pencil beams. Phys Med Biol 2005;50(3):541–61.
[15] Soukup M, Fippel M, Alber M. A pencil beam algorithm for intensity modulated proton therapy derived from monte carlo simulations. Phys Med Biol 2005;50(21):5089–104.
[16] Clasie B, et al. Golden beam data for proton pencil-beam scanning. Phys Med Biol 2012;57(5):1147.
[17] Bellinzona V, Ciocca M, Embriaco A, Fontana A, Mairani A, Mori M, et al. On the parametrization of lateral dose profiles in proton radiation therapy. Phys Med 2015;31(5):484–92.
[18] Li Y, Zhu RX, Sahoo N, Anand A, Zhang X. Beyond Gaussians: a study of single-spot modeling for scanning proton dose calculation. Phys Med Biol 2012;57(4):983–97.
[19] Bellinzona E, Ciocca M, Embriaco A, Ferrari A, Fontana A, Mairani A, et al. A model for the accurate computation of the lateral scattering of protons in water. Phys Med Biol 2016;61(4):N102–17.
[20] Würl M, Englbrecht F, Parodi K, Hillbrand M. Dosimetric impact of the low-dose envelope of scanned proton beams at a probeam facility: comparison of measurements with TPS and MC calculations. Phys Med Biol 2016;61(2):958–73.
[21] Hirayama S, Takayanagi T, Fujii Y, Fujimoto R, Fujitaka S, Umezawa M, et al. Evaluation of the influence of double and triple Gaussian proton kernel models on accuracy of dose calculations for spot scanning technique. Med Phys 2016;43(3):1437–50.
[22] Gottschalk B, Cascio E, Daartz J, Wagner M. On the nuclear halo of a proton pencil beam stopping in water. Phys Med Biol 2015;60(14):5627–54.
[23] Hall D, Makarova A, Paganetti H, Gottschalk B. Validation of nuclear models in geant4 using the dose distribution of a 177 MeV proton pencil beam. Phys Med Biol 2016;61(1):N1–10.
[24] Perl J, Shin J, Schumann J, Faddegon B, Paganetti H. TOPAS: an innovative proton Monte Carlo platform for research and clinical applications. Med Phys 2012;39(11):6818–37.
[25] Grevillot L, Frisson T, Zahra N, Bertrand D, Stichelbaut F, Freud N, et al. Optimization of geant4 settings for proton pencil beam scanning simulations using gate. Nucl Instrum Methods Phys Res, Sect B 2010;268(20):3295–305.
[26] Lin L, Kang M, Solberg T, Ainsley C, McDonough J. Experimentally validated pencil beam scanning source model in TOPAS. Phys Med Biol 2014;59(22):6859–73.
[27] Lin L, Ainsley C, Mertens T, Wilde OD, Talla P, McDonough J. A novel technique for measuring the low-dose envelope of pencil-beam scanning spot profiles. Phys Med Biol 2013;58(12):N171–80.
[28] Chanrion M, Ammazzalorso F, Wittig A, Engenhart-Cabillic R, Jelen U. Dosimetric consequences of pencil beam width variations in scanned beam particle therapy. Phys Med Biol 2013;58(12):3979–93.
[29] Lin Y, et al. Impacts of gantry angle dependent scanning beam properties on proton PBS treatment. Phys Med Biol 2017;62(2):344.
[30] Sigmund P, Schinner A and Paul H Errata and addenda: ICRU report 73 (stopping of ions heavier than helium).
[31] Yang M, Zhu XR, Park PC, Titt U, Mohan R, Virshup G, et al. Comprehensive analysis of proton range uncertainties related to patient stopping-power-ratio estimation using the stoichiometric calibration. Phys Med Biol 2012;57(13):4095–115.
[32] Luhr A, Hansen DC, Jakel O, Sobolevsky N, Bassler N. Analytical expressions for water-to-air stopping-power ratios relevant for accurate dosimetry in particle therapy. Phys Med Biol 2011;56:2515–33.